

THEORY AND MEASUREMENTS FOR TURBULENCE SPECTRA AND VARIANCES IN THE ATMOSPHERIC NEUTRAL SURFACE LAYER

ULF HÖGSTRÖM¹, J. C. R. HUNT² and ANN-SOFI SMEDMAN¹

¹*Uppsala University, Department of Earth Sciences, Meteorology, Villavägen 16, S-752 36 Uppsala, Sweden;* ²*Departments of Space, Climate Physics and Geological Sciences, University College, Gower Street, London WC1, U.K. and J.M. Burgers Centre, Delft University of Technology, the Netherlands*

(Received in final form 5 October 2001)

Abstract. Predictions from a new theory for high Reynolds number turbulent boundary layers during near-neutral conditions are shown to agree well with measurements of atmospheric surface-layer variances and spectra. The theory suggests surface-layer turbulence is determined by detached eddies that largely originate in the shearing motion immediately above the surface layer; as they descend into this layer, they are strongly distorted by the local shear and impinge onto the surface. Because the origin of these eddies is non-local, they are similar to those described in previous studies as 'inactive' turbulence. However, they are, in fact, dynamically highly active, supplying the major mechanism for the momentum transport, including upward bursting on the time scale of the larger eddies. The vertical velocity results show that the variance and the low frequency parts of spectra increase with height in the surface layer, while in the self similar (k_1^{-1}) range the streamwise low frequency components are approximately constant with height. These large-scale longitudinal eddies extend to a length Λ_s , which is equal to the boundary-layer height near the surface and increases linearly to a maximum of about three times the boundary-layer height at roughly 15 m and decreases in the upper parts of the surface layer. This lower part of the surface layer, the eddy surface layer, is the region in which the eddies impinging from layers above are strongly distorted. This new result for the atmospheric boundary layer has practical application for calculating fluctuating wind loads on structures and lateral dispersion of pollution from local sources.

Keywords: Coherent structures, Impinging eddies, Neutral surface layer, Turbulence.

1. Introduction

Certain features of the near-neutral atmospheric surface layer are observed to be not wholly consistent with Monin–Obukov theory (MO theory) nor with published measurements of laboratory non-accelerating flow over a flat plate, essentially because of non-local dynamics (Hunt and Morrison, 2000). Firstly, as observed by Högström (1990), the dimensionless vertical velocity standard deviation, σ_w/u_* (where u_* is the friction velocity) increases systematically with height above the ground, whereas MO theory predicts it to be constant. Secondly, the measured turbulent kinetic energy budget showed that dissipation, ϵ , was not in local balance with production, P , as expected. Instead it was found that $\epsilon = 1.24P$, the excess energy being brought down to the surface layer from above with the aid of the



pressure transport term. The results of Högström (1990) were confirmed in a later experiment (Högström, 1992), as well as in subsequent experiments.

Högström (1990) attempted to explain the above results in terms of the inactive turbulence concept introduced by Townsend (1961) and further elaborated by Bradshaw (1967), who also demonstrated effects of inactive turbulence in non-zero pressure gradient laboratory flow. In Bradshaw's words, Townsend's (1961) concept implies 'that turbulent motion of the inner layer consists of (i) an "active" part that produces the shear stress τ and whose statistical properties are universal functions of τ and the height above the surface, and (ii) an "inactive" and effectively irrotational part determined by the turbulence in the outer layer'. Also, according to Bradshaw (1967), there are six characteristic features of inactive turbulence:

- (i) It does not interact with the active turbulence;
- (ii) it does not contribute to the shear stress;
- (iii) it arises in the upper parts of the boundary layer;
- (iv) it is of relatively large scale;
- (v) it is partly due to the irrotational field created by pressure fluctuations in the boundary layer, and partly due to the large-scale vorticity field of the outer layer 'seen as an external stream';
- (vi) the energy of inactive turbulence is being dissipated in the layers close to the surface.

The origin and source of the 'inactive' motions in the atmospheric case, as indicated by the fifth 'feature', needs further study. In Smedman et al. (1994) airborne measurements in a near-neutral marine boundary layer showed that large-scale eddies were formed in a strong shear zone at the top of the boundary layer at nearly 1000 m and brought down to the region near the surface by the pressure transport term. The phenomena observed by Högström (1990, 1992) appear, however, to be common features of the near-neutral atmospheric boundary layer, and it is highly unlikely that the mechanism of turbulence production observed in the special marine case of Smedman et al. (1994) is generally occurring. Thus, an alternative mechanism that is directly linked to the fundamental dynamics of near-neutral boundary layers must be sought. As outlined below, such a mechanism is provided by a new theory for very high Reynolds number boundary layers proposed by Hunt and Morrison (2000) and Hunt and Carlotti (2001), based on earlier work by Townsend (1976) and Marusic and Perry (1995).

Direct numerical simulation (DNS) has revealed many features of eddy structure in moderate Reynolds number ($Re < 10^3$) boundary layers (Spalart, 1988; Robinson, 1991). Most investigators agree that in this Reynolds number range, eddies are created near the wall, deteriorate to boundary-layer turbulence and gradually grow as they move away from the wall (see also Sandham and Kleiser, 1992), but there are differing opinions about the surface instability mechanisms and the dependence on large eddies in the outer layer. However, the applicability of this model for very high Reynolds numbers has been questioned by Townsend (1976),

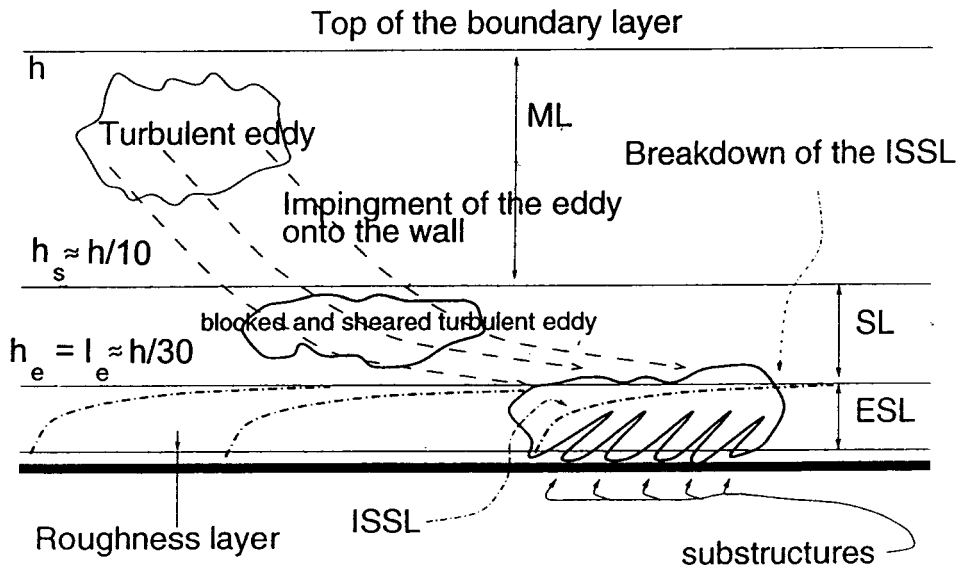


Figure 1. Sketch of a typical high Reynolds number boundary layer. Adapted from Hunt and Carloti (2001).

Mann (1994), Hunt and Morrison (2000), Hunt and Carloti (2001) and others. The latter conceptual approach was not based on a stability analysis, but on idealised analysis of turbulent eddies in shear flows near rigid boundaries by linearizing the Navier–Stokes equation with a fully turbulent state as initial conditions – the technique of Rapid Distortion Theory, RDT (Townsend, 1976). The dynamics of the very high Reynolds number turbulent boundary layer is governed by the interaction between the mean shear and detached eddies, which originate in the lower parts of the boundary layer but above the surface layer. Once such eddies are formed, whether in the interior or the flow above the wall, they persist, see Figure 1. They also originate where downburst eddies collide at the wall (or ‘anti-splats’), Perot and Moin (1995), and produce upward ejection of momentum. This process differs from the bursting instabilities near the wall that dominate the vertical momentum exchange at lower Re (Sandham and Kleiser, 1992). At low Re , where the shear $\partial U/\partial z$ is stronger in the upper part of the surface layer, the lower part of the surface layer is sheltered from the energetic eddies in the upper layer (Hunt and Durbin, 1999). At high Re the impinging eddies are stretched out and replicate themselves in the intense local shear near the surface in trains extending a distance of order h , as ‘cats paws’ or honami waves. This mechanism is similar to that of the wake of a jet or plume in a crossflow where eddies form downwind as a result of shed vorticity (e.g., Coelho and Hunt, 1989). These extended surface eddies, which are strongly affected by the surface friction at the ground, are significant in the *eddy surface layer* whose thickness h_e is less than that of the surface layer, h_s (Figure 1),

h_e being 2–4% of the boundary-layer thickness, i.e., about $h_s/3$ or typically about 15 m.

In Section 2, the predictions of the theory are presented and in Section 3 the various predictions are tested against measurements in the near-neutral atmospheric surface layer.

2. Theory

2.1. GENERAL CONSIDERATIONS AND A PREDICTION FOR THE VERTICAL VELOCITY VARIANCE AND THE u - w CORRELATION

The turbulent boundary layer of depth h is conveniently sub-divided into a surface layer of depth $h_s = O(h/10)$, where turbulence is in approximate local equilibrium, because production by strong mean shear approximately balances the rate of dissipation, ϵ , i.e., $u_*^2(dU/dz)/\epsilon \approx 1$ (note, however the result of Högström, 1990 and 1992 that pressure transport in the neutral surface layer amounts to as much as 24% of the local production) and an upper layer where turbulence is not in equilibrium and with considerably weaker shear, and the energy and the dissipation rate are smaller, so that $u_e^2(dU/dz)/\epsilon \ll 1$, u_e being a typical eddy velocity scale of order the friction velocity. For high enough values of the turbulent Reynolds number, $Re_\tau = u_e L_e / \nu \gg 10^4$, where ν is kinematic viscosity, and L_e an eddy length scale above the surface layer, the turbulence in the upper layer is generated more by the local shear than by diffusion from the surface layer. But the turbulence is not in equilibrium, because the turbulent energy diffuses or propagates outward to the top of the layer. The shear generated eddy motions also propagate downward to the surface layer where they are further distorted by the intense shear and also impact on the ground. The former process leads to groups of elongated sloping eddies that replicate themselves as ‘cats paws’ and honami waves (Hunt and Carloti, 2001). This leads to amplified eddies and amplified horizontal components. With or without shear, blocking at the surface creates a potential flow component that modifies the vertical velocity, where the variance σ_w^2 is given, according to RDT calculations (Hunt, 1984; Mann, 1994), by

$$\sigma_w^2 \approx u_e^2 \left(\frac{z}{L_e} \right)^{2/3}. \quad (1)$$

The total vertical velocity variance in the surface layer is the sum of the contribution of the blocked eddies of the upper layer, Equation (1), and that of small-scale turbulence created near the surface, which scales on u_* , giving for the total variance

$$\sigma_w^2 = \alpha u_*^2 + \beta u_e^2 \left(\frac{z}{L_e} \right)^{2/3}, \quad (2)$$

where $\alpha \sim 1$, $\beta \sim 1$, $u_e \sim u_*$, so that

$$\frac{\sigma_w^2}{u_*^2} \approx 1 + \left(\frac{z}{L_e} \right)^{2/3} \quad (3)$$

and where L_e is expected to scale with u_*/f_c and to be $O(h_s)$ or $O(h_e)$.

This combination of local shear plus blocking of large-scale eddies also occurs in the unstable atmospheric boundary layer when there is both a mean horizontal wind and significant thermal convection (Panofsky et al., 1977; Hunt, 1984; Hunt et al., 1989).

For low Re flow, where the mean velocity gradient is much greater at the top of the surface-layer, the shearing motion ‘shelters’ or decorrelates the surface-layer eddies from those of the outer turbulence (Hunt et al., 1989). Then the second term in Equation (3) is absent.

Because the blocking effect reduces w but increases u , it affects the correlation coefficient between the vertical and horizontal velocity components, defined by

$$r_{uw} = \frac{\overline{u'w'}}{\sigma_u \sigma_w} = -\frac{u_*}{\sigma_u} \frac{u_*}{\sigma_w}, \quad (4a)$$

where σ_u^2 is the variance of the longitudinal wind component (see Section 3.2 for Equation (4b)). According to the shear-free boundary layer (SFBL) RDT calculations of Hunt (1984),

$$\Delta\sigma_w^2 = \Delta\sigma_u^2 + \Delta\sigma_v^2, \quad (5)$$

where $\Delta\sigma_w^2$ is the difference between the vertical velocity variance at the top of the surface layer, i.e., at $z = h_s$, and that due to blocking at a given height $z < h_s$ given by (3). In a sheared boundary layer, the formula (5) does not strictly apply, because the extra straining near the ground increases $\Delta\sigma_u^2$, $\Delta\sigma_v^2$ to a greater extent than simply by blocking, as shown in Section 2.3 (see also the measurements in Section 3.2). As Hunt and Carlotti (2001) show theoretically, the blocking effect dominates the vertical component, but not the horizontal components.

2.2. PROPERTIES OF VERTICAL VELOCITY SPECTRA AND u - w COSPECTRA

RDT for SFBL shows (Hunt, 1984) that the vertical velocity energy reduction by blocking expressed by (3) is very scale selective, large eddies being more strongly blocked than smaller eddies; for eddies with horizontal wavenumber $k_1 < 1/z$, the corresponding spectrum $F_{33}(k_1)$ should obey

$$F_{33} = \alpha_3 \epsilon^{2/3} z^{5/3}, \quad (6)$$

where α_3 is the transverse Kolmogoroff constant = 0.67. For comparison with atmospheric spectra, Taylor’s hypothesis is employed, i.e., it is assumed that

$k_1 = 2\pi n/\bar{u}$, where n is frequency and \bar{u} mean wind speed. Multiplying Equation (6) with k_1 and making the expression dimensionless by dividing with u_*^2 gives

$$\frac{nS_w(n)}{u_*^2} = \lambda f, \quad (7a)$$

where

$$\lambda = \frac{2\pi\alpha_3\varphi_\epsilon^{2/3}}{\kappa^{2/3}}, \quad (7b)$$

and f is the non-dimensional frequency, nz/\bar{u} , κ the von Karman constant = 0.40 and $\varphi_\epsilon = \epsilon\kappa z/u_*^3$ the non-dimensional dissipation rate, found by Högström (1990, 1992) to be 1.24 in neutral conditions. Using these numerical values, gives a predicted value of $\lambda = 9$.

By contrast, where the wavenumbers are high enough, the mean shear and blocking effect are negligible and the turbulence is locally homogeneous and isotropic, so that the Kolmogoroff inertial subrange prediction is valid, i.e.,

$$\frac{nS_w(n)}{u_*^2} = \frac{\alpha_3}{(2\pi\kappa)^{2/3}}\varphi_\epsilon^{2/3}\left(\frac{nz}{\bar{u}}\right)^{-2/3} = \frac{\alpha_3}{(2\pi\kappa)^{2/3}}\varphi_\epsilon^{2/3}f^{-2/3}. \quad (8)$$

Thus, the dimensionless vertical velocity spectrum is a function only of the dimensionless frequency f for low frequencies (Equation (7)) as well as for high frequencies (Equation (8)).

For the u - w cospectrum Hunt and Carlotti (2001) show that a similar transition occurs. For low frequencies it is predicted that

$$\frac{nCo_{uw}(n)}{u_*^2} = \beta f, \quad (9)$$

where the constant $\beta \sim \lambda$. For high frequencies, the corresponding prediction (Wyngaard and Coté, 1972) is

$$\frac{nCo_{uw}(n)}{u_*^2} = \chi f^{-4/3}, \quad (10)$$

where χ is a constant.

2.3. PREDICTIONS FOR THE LONGITUDINAL VELOCITY SPECTRUM

In the lowest part of the surface layer or eddy surface layer, where $z < h_e$, the low wavenumber spectrum for the longitudinal wind component is strongly distorted by the blocking, intense shearing and surface scraping mechanisms. It is not only quite different from its form for the vertical component, but it also differs from its form in the bulk of the surface layer (Hunt and Morrison, 2000; Mann, 1994). Physical and dimensional analysis shows that the $nS_u(n)$ spectrum exhibits several characteristic spectral regimes (Perry et al., 1986):

- (i) for $k_1 \gg z^{-1}$, the Kolmogoroff inertial range, with spectral slope $-2/3$;
(ii) for $\Lambda_s^{-1} < k_1 \ll z^{-1}$ there is the surface eddy range; for $\Lambda_s^{-1} \ll k_1$, where Λ_s is the largest horizontal eddy, there is the self similar range where $F_{11}(k_1) \propto u_*^2 k_1^{-1}$, or, in frequency representation:

$$nS_u(n)/u_*^2 \approx \gamma, \quad (11)$$

where $\gamma \sim 1$,

- (iii) for very low wavenumbers where $k_1 < \Lambda_s^{-1} \sim u_*/hU$, $F_{11}(k_1 \rightarrow 0) \propto u_*^2 \Lambda_s$, or in frequency form,

$$nS_u(n)/u_*^2 \propto n\gamma. \quad (12)$$

Ranges (i)–(iii) represent boundary-layer turbulence. Range (ii) only exists in the eddy surface layer. But at even lower frequencies, ‘one-hour’ mean flow fluctuates. This is a result of the mesoscale unsteady quasi two-dimensional motion that is found to be universally present in the troposphere and lower stratosphere (Gage and Nastrom, 1986; Höögström et al., 1999). This leads to a fourth range in the spectra where

- (iv) spectral energy increases with decreasing frequency.

Ranges (iii) and (iv) are separated by a more or less pronounced ‘spectral gap’ (Panofsky, 1969; Smedman-Högström and Höögström, 1975). Note that very close to the surface, where $z \ll h_e$, the large-scale horizontal fluctuations are reduced by surface friction. This rapid variation with height of the large-scale horizontal eddies is because very close to the ground the surface friction forces acting on each eddy impinging from above damp out longer eddies at a greater height than smaller eddies. This rapid variation with height of the large-scale horizontal eddies is because very close to the ground the surface friction acts to generate an internal boundary layer in each eddy. These are thicker for larger eddies and thinner for smaller eddies. But large eddies move faster and this may explain why the spectral energy at a given height increases with decreasing frequency.

In the inertial subrange (i) the relation for the non-dimensional spectrum $nS_u(n)/u_*^2$ is the same as the corresponding equation for the vertical component, Equation (8), except for a constant factor, $\alpha_1 = (3/4)\alpha_3 = 0.52$. Thus in this range, $nS_u(n)/u_*^2$ is a function of the non-dimensional frequency f only. Note that this is not the case for spectral ranges (ii) and (iii). The lower frequency limit n_l of range (ii) is obtained from the intersection of spectral ranges (ii) and (iii), determined by the wavelength Λ_s . For (iii) the prediction (Perry et al., 1986; Hunt and Morrison, 2000; Hunt and Carlotti, 2001) is

$$k_1 F_{11}(k_1)/u_*^2 = nS_u(n)/u_*^2 = \Lambda_s n \bar{u}, \quad (13)$$

where Λ_s is of the order of h , the boundary-layer depth. Since $h \sim u_*/f_c$, $\Lambda_s = Au_*/f_c$. Thus, rewriting Equation (13) gives

$$nS_u(n)/u_*^2 = A \frac{u_* n}{f_c \bar{u}} \quad (14)$$

for $n < n_l$, where $A(z)$ is a parameter to be determined from the measurements. But at the lower frequency limit of the k_1^{-1} range, where $n = n_l$, since $nS_u(n)/u_*^2 \approx 1$, the vertical variation of A is determined to be

$$A = f_c \frac{\bar{u}}{u_*} \frac{1}{n_l} = f_c \frac{1}{\kappa} \left(\ln \frac{z}{z_0} \right) \frac{1}{n_l}, \quad (15)$$

using the observed logarithmic wind profile for $\bar{u}(z)$.

Note that above the eddy surface layer the length scale Λ_s of the horizontal structures decreases. Thus in the bulk of the surface layer, $h_e < z < h_s$, there is no self-similar k_1^{-1} range, only a transition between the inertial range and the 'flat' low frequency range.

An approximate expression for σ_u^2/u_*^2 can be obtained in the following way. Assume that there is no intermediate range between range (i) and (ii), i.e., extend the inertial subrange to the frequency n_0 where

$$nS_u(n)/u_*^2 = 1 = \frac{\alpha_1}{(2\pi\kappa)^{2/3}} \varphi_\epsilon^{2/3} \left(\frac{n_0 z}{\bar{u}} \right)^{-2/3},$$

so that, with numerical values given above: $n_0 = 0.185(\bar{u}/z)$. Also, assume that the transition between range (ii) and (iii) occurs, without any intermediate range, at $n = n_l$, which is given by Equation (15). Denote the integral over the inertial subrange $I_1 = \int_{n_0}^{\infty} [S_u(n)/u_*^2] dn \approx 1.5$. The corresponding integral over range (ii) becomes:

$$I_2 = \ln \frac{n_0}{n_l} = \ln \frac{0.46u_* A \kappa}{zf_c}.$$

For range (iii): $I_3 \approx 1$. Finally,

$$\frac{\sigma_u^2}{u_*^2} \approx I_1 + I_2 + I_3 \approx 2.5 + \ln \frac{0.46u_* A \kappa}{zf_c}. \quad (16)$$

The measurements (see Section 3) show that Equation (16) is approximately valid in the surface layer down to at least 1.6 m above the ground. With A finite, Equation (16) gives, however, that σ_u^2/u_*^2 is infinite at the surface, so that there must be a layer $z \ll h_e$ in which this expression is not valid.

3. Validation against Atmospheric Near-Neutral Measurements

3.1. THE PREDICTIONS FOR THE VERTICAL VELOCITY VARIANCE

3.1.1. *The Data*

The prediction, Equation (3), has been tested on well-documented near neutral atmospheric surface-layer data from 10 sites, see Table I. The data have all been chosen to represent near-neutral conditions. In the selection of ‘near-neutral data’ the stability criterion has been: $-0.1 < z_t/L < 0.1$, where z_t is the highest measuring level for each site ($z_t \geq 10$ m, except at site (5) where $z_t = 6$ m). As shown in Högström (1990, 1992), the characteristic height variation in σ_w/u_* was observed in a stability interval of at least this magnitude. A general criterion of stationarity was also imposed. All measuring sites are flat but dynamically rough, and with a roughness length z_0 varying from about 10^{-4} m (open sea) to about 0.5 m (pine forest). The measurements are all in the constant flux layer but represent heights ranging from 1.6 m to about 30 m. In fact, most of them, except for two levels at site 6, one level at site 7 and two levels at site 10, are effectively in the eddy surface layer. Out of the 10 data sets, 8 are from experiments carried out in various parts of Sweden by the Uppsala group. The two remaining data sets, which are taken from the open literature, represent oceanic conditions. Unfortunately, most widely spread micrometeorological data sets (such as the Kansas data, Haugen et al., 1971 or the Australian data, e.g., Dyer, 1974) represent land summertime fair weather mid-latitude conditions, which means that neutral conditions occur only briefly during morning and evening transition periods, making these data sets unsuitable for the present analysis. Reviews of other spectral data are given by Hunt and Morrison (2000).

3.1.2. *Test of Height Variation*

In testing Equation (3), it is assumed that the basic length scale is u_*/f_c (as obtained for eddy motions in a rotating neutral flow) and further that L_e is proportional to this scale, because it determines the eddy motion in the upper layer. In Figure 2 $y = \sigma_w^2/u_*^2$ has been plotted against $x = 10^3(zf_c/u_*)^{2/3}$. It is clear from the figure that the non-dimensional vertical velocity variance increases with height in accordance with Equation (3). The data points from the lowest measuring levels (1.6 and 3 m) deviate, however, from the general pattern in an interesting way. According to Hunt and Carlotti (2001), although the forms of impinging eddies change in the thin eddy surface layer (see Section 2), the blocking mechanism itself is still significant. However, as a result of the eddies being distorted when they encounter the ground surface, Figure 1, their vertical velocity is being gradually reduced with decreasing height near the surface. This explains why, as Figure 2 indicates, the magnitude of the blocking term of Equation (3) decreases where $z \ll h_e$, i.e., for the measurements at 1.6 and 3 m. Note that these measurements were made with the MIUU turbulence instrument, i.e., with tiny hot-film probes

TABLE I

Measuring sites for test of σ_w/u_* variation with height. The first column gives the name of the site and reference to the source (listed below the table). The second column gives general characteristics of the site, the third column measuring heights and the last column the latitude of the site.

Name and reference	Characteristics	Heights (m)	Latitude
Lövsta ^a	Agricultural	3, 6, 13	59° N
North Sea ^b	Ocean	10	53° N
Bottenviken ^c	Sea ice	2, 4, 10	64° N
Marsta ^d	Agricultural	10	59° N
Laban's mills ^e	Heath	1.6, 3, 6	57° N
Jädraås ^f	Pine forest	14, 26, 32*	61° N
Vänernsberg ^g	Agricultural	10, 23	58° N
Näsudden ^h	Juniper heath	11	57° N
Sable island ⁱ	Ocean	10	44° N
Östergarnsholm ^j	Ocean	8, 16, 24	57° N

*These heights are $(z - d)$, with $d =$ zero plane displacement = 8 m.

^aHögström (1990).

^bFrom figure in: Geernaert and Plant (1990).

^cData from three sites on the ice of the Bothnian Bay. Annual Report, EU-project BASIS (2000).

^dJohansson et al. (2001).

^eData from the 'Laban's mills' site, Högström (1992).

^fData from the Jädraås site, cf. Högström et al. (1989).

^gData from the Vänernsberg site, cf. Smedman (1991a).

^hData from the Näsudden site, cf. Smedman (1991b).

ⁱSmith and Banke (1975).

^jData from the Östergarnsholm site, cf. Smedman et al. (1999).

confined to a small volume (roughly 5 mm cube, cf. Högström, 1982), so that the measurements were not contaminated by finite path length averaging effects (which might have been the case if a sonic anemometer had been used at such low heights).

Based on the above concept, L_e is proportional to u_*/f_c . Regression of the data in Figure 2 gives, $L_e \approx 10^{-2}u_*/f_c$. Taking the boundary-layer height $h = 0.3u_*/f_c$, implies that $L_e \approx h_e$, i.e., the height of the eddy surface layer.

This statement implies that the length scale is a function of latitude (ϕ). By taking data from sites with widely different latitude, this can be tested. Thus, in Figure 2, there are data from one site at 44° N (no. 9, Sable Island) and one at 64° N (no. 3, Bottenviken). Making regression with those two data sets only, gives a very similar regression expression as that obtained with the entire data set and with a correlation coefficient $r = 0.75$ for the case when ϕ is allowed to vary. If,

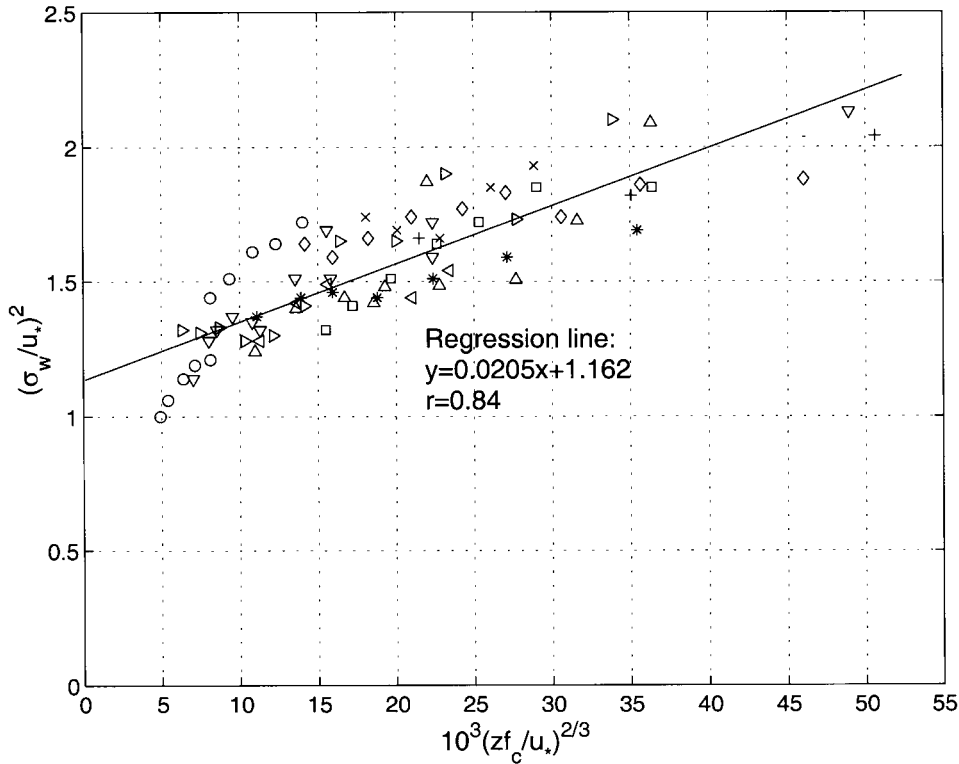


Figure 2. Normalized vertical velocity variance plotted against $10^3(zf_c/u_*)^{2/3}$. Symbols denote the sites; numbers in parenthesis refer to Table I: ∇ , Lövsta (1), agricultural, 3 levels; *, North Sea (2), ocean; $>$ Bottenviken (3), ice, 3 levels; \times , Marsta (4), agricultural; \circ , Laban's mills (5), heath, 3 levels; \diamond , Jädraås (6), pine forest, 3 levels; $+$, Vänersborg (7), agricultural, 2 levels; square, Näsudden (8), juniper heath; $<$, Sable Island (9), ocean; \triangle , Östergarnsholm (10), ocean, 2 levels. Note, that each symbol represents the mean of a number of measurements from each particular site and height.

instead, a mean value for ϕ is taken, r decreases to 0.61, implying that the explained variance has dropped from 0.56 to 0.37.

From the above analysis it is clear that the observed height variation of $(\sigma_w/u_*)^2$ is in close agreement with the prediction (3). Note that, as stated at the beginning of Section 3.1.1, the data sets used in this analysis contain observations representing slightly unstable as well as slightly stable conditions. A separate analysis is presented in Högström (1990) to show that the height variation of $(\sigma_w/u_*)^2$ observed at the Lövsta site is virtually the same for the slightly unstable stability range, $-0.1 \leq z/L < 0$, and for the corresponding slightly stable range, $0 \leq z/L \leq 0.1$. Thus, the suggestion (made by a referee) that the observed height variation might be due to convective motions can be ruled out as an alternative explanation.

As mentioned at the onset of Section 3.1.2, the use of u_*/f_c as a basic scaling length in the present analysis is a consequence of the theory for turbulence in

rotating flow. The analysis presented above supports this choice of length scale. For the truly neutral atmospheric boundary layer (NABL) this theory predicts the depth of the boundary layer h to be proportional to this length scale, the constant of proportionality being about 0.3. Often in reality other factors, such as a slight deviation from neutrality of the bulk of the boundary layer, may strongly influence the actual value of h . This fact does not invalidate the use of u_*/f_c as a scaling parameter for the turbulence in the lower parts of the actual NABL. Also, $h = 0.3u_*/f_c$ is used as a rough estimate of the depth of the NABL in the present analysis.

3.2. THE CORRELATION COEFFICIENT BETWEEN u AND w

Taking the square of Equation (4), we have the following relation

$$r_{uw}^2 = \left(\frac{u_*}{\sigma_w}\right)^2 \left(\frac{u_*}{\sigma_u}\right)^2. \quad (4b)$$

In low Reynolds number flat plate laboratory experiments, e.g., Monin and Yaglom (1971), r_{uw} is found to be -0.5 , i.e., $r_{uw}^2 = 0.25$. As Högström (1990) pointed out, this contrasts to values reported from the near-neutral atmospheric surface layer, where r_{uw} is found to be in the range -0.25 to -0.35 , so that r_{uw}^2 is between 0.06 and 0.12. Högström (1990) interpreted this as an effect of inactive turbulence, which is supposed to make a contribution to the variances σ_u^2 and σ_w^2 but not to the shearing stress u_*^2 .

Data from the ‘Laban’s mills’ site (Högström, 1992), have been used to test the variation of r_{uw}^2 with height. The result of regression analysis is that r_{uw}^2 varies approximately in agreement with the inverse of the observed variation of $(\sigma_w/u_*)^2$, thus implying that $(\sigma_u/u_*)^2$ is virtually constant with height. The result also implies that r_{uw} varies systematically with height in the neutral surface layer, being about -0.35 near the surface and about -0.25 at 14 m. However, as noted in Section 2, the increase with height of the vertical component is expected to be approximately balanced by a corresponding decrease in the variance of the horizontal components, Equation (5). Taking values of $(\sigma_w/u_*)^2$, and r_{uw}^2 at a height z within the surface layer leads to $(\sigma_u/u_*)^2 \approx 8$. According to Equation (5), the observed 100% increase in vertical velocity variance across the surface layer would correspond to only about 6% relative decrease of due to blocking. Equation (16) shows, however, that the actual decrease across the surface layer ($h_e/10 < z < h_s$) is likely to be about 15%. This disagreement with Equation (5) is, however, not surprising, considering the simplifications underlying its derivation. Nevertheless, a 15% decrease in $(\sigma_u/u_*)^2$ corresponds to only about 7% decrease in σ_u/u_* . Since such a small variation is within the scatter of the measured data, it is likely to escape detection. Therefore the model is consistent with the experimental result that $(\sigma_u/u_*)^2$ is approximately height constant within the measurement accuracy. The observed constant value for $(\sigma_u/u_*)^2 = 8$, is about 50% larger than that observed in zero-pressure flat plate laboratory studies at relatively low Reynolds number. As

discussed in Section 3.4, this enhancement of the magnitude of the longitudinal component energy is due to a spectral extension at the low frequency end, which can be explained as a result of large, elongated eddies scraping along the ground (cf. Figure 1), cf. Section 4.

4. Vertical Velocity Spectra and u - w Cospectra

According to the predictions in Section 2, the normalized vertical velocity spectrum, $nS_w(n)/u_*^2$ should be a function of the normalized frequency $f = nz/\bar{u}$ in the atmospheric surface layer. Figure 3 shows a mean spectrum for the three measuring levels (1.6, 3 and 6 m) from the site ‘Laban’s mills’ (Högström, 1992) – data represented by the circles. The two lines drawn are the predictions, Equations (7) and (8), which are expected to be valid in the low frequency range and in the inertial subrange respectively. They are seen to make an excellent fit to the data. The same result (not shown here) is obtained with data from the three measuring levels (3, 6 and 14 m) at the Lövsta site (Högström, 1990). Plots of individual spectra from both sites show that the data points scatter around the mean curve given by the circles in Figure 3, without any systematic variation with height. Also included in this figure is the widely quoted vertical velocity spectral plot from the Kansas experiment (Kaimal et al., 1972) – given as the dashed curve. It is seen to have roughly the same general trend in the low-frequency range as that predicted by Equation (7), but the Kansas curve is low by a factor of about 3, perhaps because the data were filtered to avoid the influence of mesoscale low-frequency fluctuations in the horizontal wind, cf. Section 3.4.

According to the predictions of Equations (9) and (10) in Section 2, the non-dimensional cospectrum between the longitudinal and the vertical component, $nCo_{uw}(n)/u_*^2$, is a function of the dimensionless frequency $f = nz/\bar{u}$ as well, for low and high frequencies respectively. Data from three measuring levels (3, 6 and 14 m) from the Lövsta site (Högström, 1990) have been used to test these predictions and to determine the coefficient β . Plots of the individual non-dimensional spectra as a function of dimensionless frequency (not shown here) show that the data collapse with no systematic height dependence. The low-frequency prediction (9) is supported by the data, giving $\beta = 19 \pm 9$ (s.d.), to be compared with the prediction of Hunt and Carlotti (2001), $\beta \sim \lambda = 9$. For the exponent in the high-frequency range (cf. Equation 10), the measurements give: -1.24 ± 0.14 (s.d.), which is close to the prediction -1.33 .

4.1. LONGITUDINAL VELOCITY SPECTRA

Figure 4 shows the mean normalized longitudinal velocity spectrum $nS_u(n)/u_*^2$ as a function of frequency n in the range $4 \times 10^{-5} \text{ Hz} < n < 10 \text{ Hz}$. It has been computed as a mean from measurements at three levels ($z = 1.6, 3$ and 6 m) from three

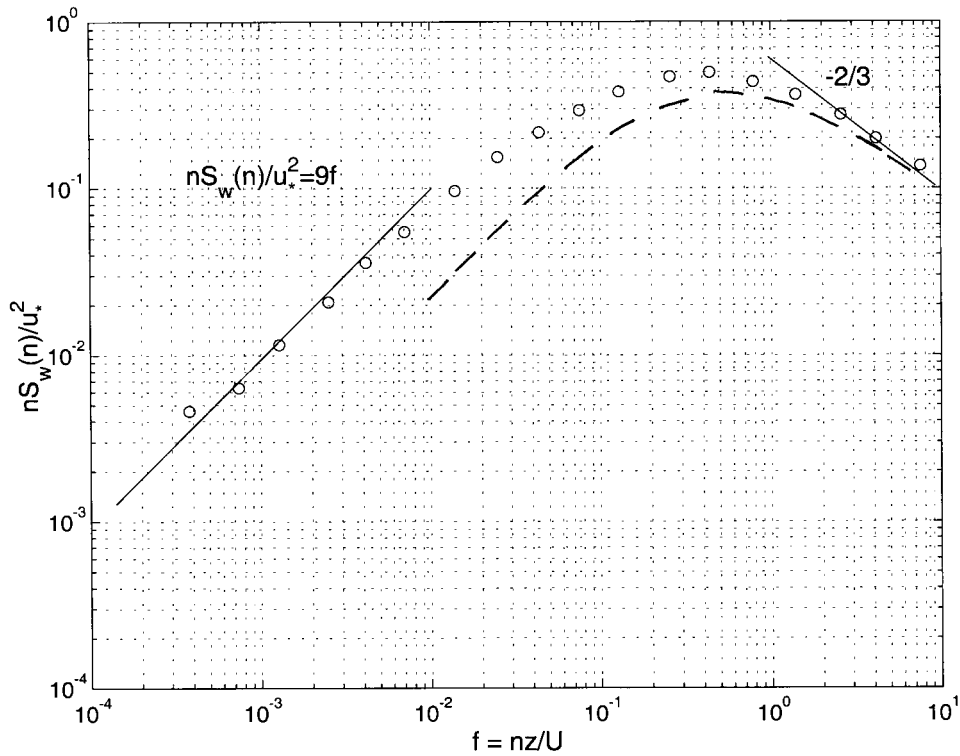


Figure 3. Normalized spectrum of vertical velocity plotted against normalized frequency $f = nz/\bar{u}$, the circles. Mean values from three measuring levels at the Laban's mills site (Högström, 1992). The line to the left is Equation (7), with $\lambda = 9$; the line denoted '-2/3' is the inertial subrange prediction (8). The dashed curve is taken from Kaimal et al. (1972).

periods of respectively 13-hour, 8-hour and 4-hour duration of reasonably steady-state near-neutral measurements at the 'Laban's mills' site (Högström, 1992). It shows clearly the existence of the four spectral regimes outlined in Section 2: (i) the inertial subrange, with a $-2/3$ spectral slope; (ii) a range where $nS_u(n)/u_*^2 \approx \gamma$, with $\gamma \approx 1$ (Equation (11)); (iii) a range where $nS_u(n)/u_*^2 \propto n$ (Equation (12)); (iv) a range where $nS_u(n)/u_*^2$ increases with decreasing frequency. The transition from range (iii) to (iv) appears rather abruptly at around $n \approx 7 \times 10^{-4}$ Hz, (i.e., a period of 30 minutes) where there is a pronounced minimum in the curve: the spectral gap.

Figure 4 is illustrative because it shows all four spectral ranges in one plot. However, as a result of the averaging procedure, it hides certain important features, in particular the variable extension (in this representation) of range (ii). Figure 5 shows a typical example of an individual spectrum from 3-m height at the Lövsta site (Högström, 1992) (the circles), with ranges (i)–(iii). This specific spectrum, as well as all analyzed spectra, have a range with $nS_u(n)/u_*^2 \approx 1$, so that $\gamma \approx 1$. This is consistent with many published data from turbulent pipe flow, e.g., Perry

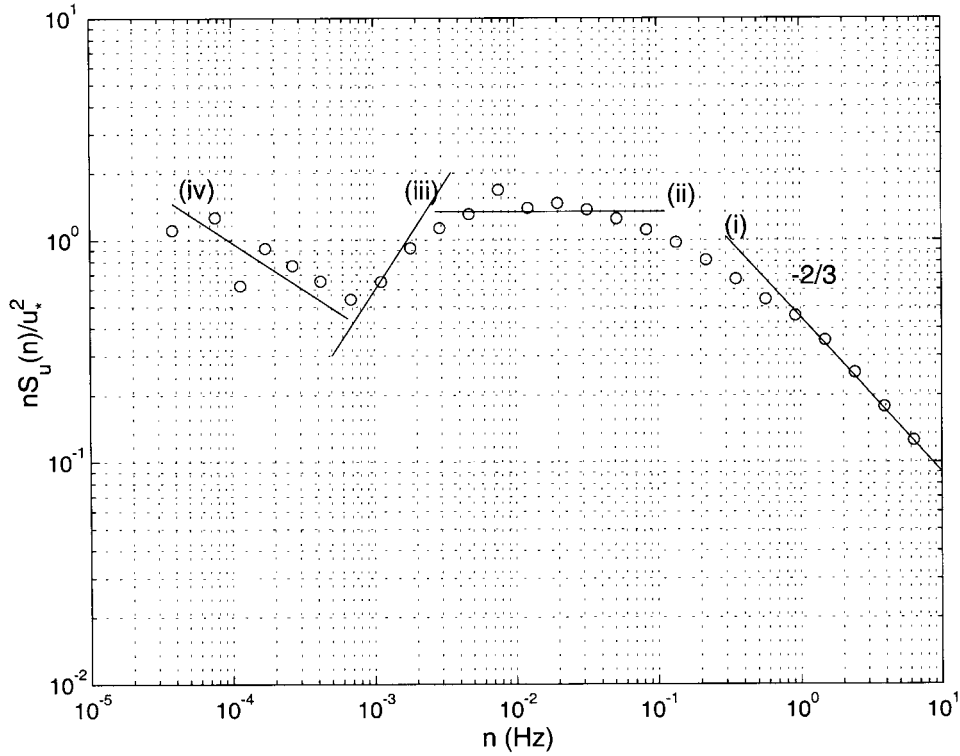


Figure 4. Normalized mean longitudinal velocity spectrum plotted against frequency based on measurements at the 'Laban's mills' site (Högström, 1992) during three periods of respectively 13-hour, 8-hour and 4-hour duration and three levels. The lines denoted (i) through (iv) are spectral ranges discussed in the text.

and Abell (1977). Such scaling was recently also reported from the atmosphere, Katul and Chu (1998), showing extensive ranges corresponding to $nS_u(n)/u_*^2 \approx 1$ from three sites with varying types of roughness. Note that the range of frequencies in this ' k_1^{-1} ' self-similar range decreases with height z , as schematically indicated by the dashed lines in Figure 5, and with wind speed. This is predicted by the theoretical discussion in Section 2 when $z \leq h_e$, where h_e is the thickness of the eddy surface layer. The inertial subrange (i) scales with f . Examination of the individual spectra shows that this is also the case for the upper frequency limit of range (ii), i.e., $n_u = f_u \bar{u}/z$, where $f_u \approx \text{constant}$, so that n_u decreases with increasing height and increases with increasing wind speed. The lower frequency limit n_l is obtained from the intersection of spectral ranges (ii) and (iii), determined by the wavelength Λ_s of the largest eddies. For (iii) the prediction, Equation (13), is:

$$k_1 F_{11}(k_1)/u_*^2 = nS_u(n)/u_*^2 = \Lambda_s n / \bar{u},$$

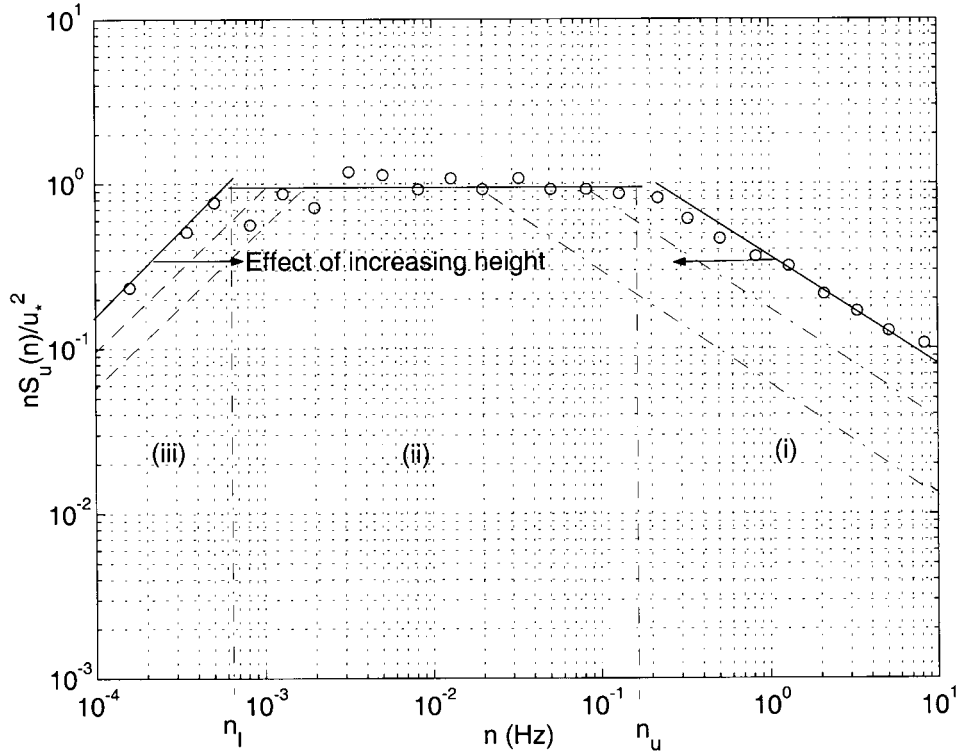


Figure 5. Example of 30-minute normalized longitudinal near-neutral spectrum at 3 m, from the Lövsta site (Högström, 1990), circles. Full lines show the corresponding spectral ranges (i)–(iii). Dashed lines indicate schematically how these ranges vary with height. n_u and n_l are the upper and lower frequency limits respectively of range (ii).

where $\Lambda_s = Au_*/f_c$ and, according to Equation (15),

$$A = f_c \frac{\bar{u}}{u_*} \frac{1}{n_l} = f_c \frac{1}{k} \left(\ln \frac{z}{z_0} \right) \frac{1}{n_l}.$$

Therefore the frequency ratio n_u/n_l is maximum, about 50, at around 5-m height and decreasing to about 1 at the top of the eddy surface layer.

The parameter A has been evaluated from three data sets: ‘Laban’s mills’ (Högström, 1992), Lövsta (Högström, 1990) and Östergarnsholm (Smedman et al., 1999), and mean values for each level and site have been plotted as a function of height in Figure 6. The result means that the length scale $\Lambda_s = Au_*/f_c$ is very large throughout the eddy surface layer but increases linearly with height, where the large eddies scrape along the ground. With the height of the boundary layer, $h \approx 0.3u_*/f_c$, we obtain: at 1.6 m, $\Lambda_{\max} \approx h$ and at 15 m, $\Lambda_{\max} \approx 3h$. In Figure 6 it is clear that the 24-m data point deviates considerably from the trend of the other measurements. This is consistent with n_u/n_l decreasing below 1.0 above this level. It is concluded that the 24-m level at the marine site Östergarnsholm is above

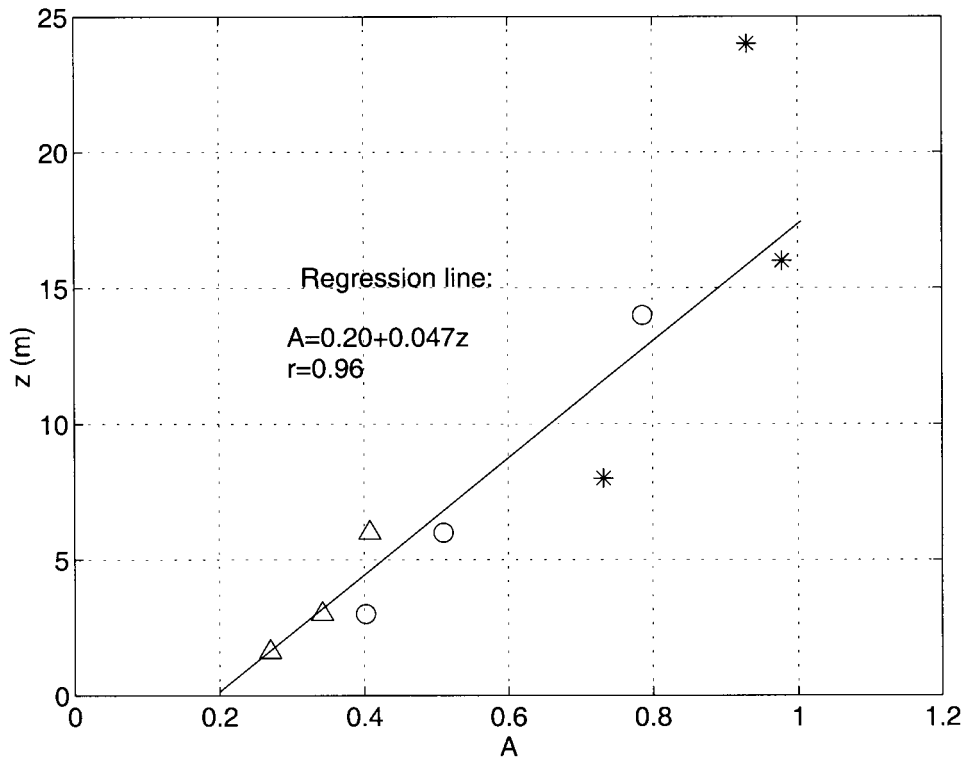


Figure 6. The scale parameter A of the expression $\Lambda_{\max} = Au_*/f_c$ plotted against height. Data from: 'Laban's mills' (Högström, 1992), Δ ; Lövsta (Högström, 1990), \circ ; Östergarnasholm (cf. Smedman et al., 1999), $*$. Note that each symbol represents a mean over many measurements from each site and measuring height.

the eddy surface layer. Above the eddy surface layer the scale Λ_s decreases again, as illustrated by the strong wind case from the marine site Sprogö, Mann (1994). A spectrum is given for a 6-hour period with a mean wind speed of 22 m s^{-1} at 70-m height. It shows no evidence of a region with constant normalized spectrum (i.e., range (ii)), and it has a maximum wavelength approximately equal to $\Lambda_s \approx h$, i.e., $A = 0.3$. These results show that for horizontal velocity fluctuations, the length scales are greatest in the upper parts of the eddy surface layer.

The existence of very large-scale energy in near-neutral surface-layer u spectra is evident in the studies reviewed by Davenport (1961) and has been used in most wind engineering calculations since then. His spectra differed greatly from the much quoted Kansas u spectra, which were plotted as a function of non-dimensional frequency $f = nz/\bar{u}$, Kaimal et al. (1972). In this representation, the non-dimensional near-neutral spectra from measurements at 5.66, 11.34 and 22.6 m are represented by a single curve with a pronounced maximum at $f = 5 \approx 10^{-2}$, corresponding typically (with $\bar{u} \approx 2z$) to $n = 10^{-1}$ Hz. This is near $n = n_u$ in Figure 5. However, at $f = 5 \times 10^{-3}$, the normalized Kansas spectrum has dropped

from its maximum value of 1.0 to about 0.3. This strongly contrasts with Figure 5, which shows that spectral energy at 3 m remains at around 1.0 for two decades in n . As mentioned in connection with the discussion of the corresponding Kansas plot for the vertical velocity, Figure 3, it is probable that low-frequency energy was deliberately not plotted in the Kansas analysis, in order to avoid having to consider low-frequency mesoscale fluctuations.

Thus, using Figure 4, boundary-layer turbulence and mesoscale fluctuations can be distinguished objectively by their different contributions to the two spectral ranges denoted by (iii), where spectral energy increases linearly with *increasing* frequency, and (iv), where spectral energy increases with *decreasing* frequency. The separation point which, according to Figure 4, appears at around 7×10^{-4} Hz, is identical to the spectral gap. Note, that the exact position of the spectral gap varies with height, cf. the variation of the range (iii) in Figure 5.

5. Discussion

Observations of ‘very large-scale motions’ (VLSMs) in turbulent pipe flow at high Reynolds number were reported by Kim and Adrian (1999). They found a linear variation in size of the VLSMs with distance from the wall, with a sudden drop in size above the top of the logarithmic layer. The general form of the longitudinal spectra reported by Kim and Adrian (1999) in this layer is also similar to that obtained here, with clearly defined ranges (i)–(iii). They argued that their spectrum would result from a superposition of two independent spectra representing different mechanisms. In Figure 7 an example of a measured normalized atmospheric longitudinal spectrum, $nS_u(n)/u_*^2$ has been plotted in the same representation as that employed by Kim and Adrian (1999), i.e., with spectral energy on a linear scale against frequency on a logarithmic scale. Also plotted in this figure is the corresponding normalized vertical velocity spectrum, $nS_w(n)/u_*^2$ and the cospectrum $nCo_{uw}(n)/u_*^2$. In order to remove the relatively large scatter in the original data in a linear representation, spectral data have been taken from subjectively drawn smooth curve fits to the original plots in log–log representation. In Figure 7 an attempt has been made to sketch two possible spectral distributions, the sum of which is the observed longitudinal velocity spectrum. Kim and Adrian (1999) found in their data that there was generally a maximum in the observed longitudinal velocity spectrum at the low frequency end of the flat spectral range. This feature is also often observed in our individual atmospheric spectra, although not in the particular example shown in Figure 7. Indeed, there is an indication of such a maximum at $n = 7 \times 10^{-3}$ Hz in the mean spectrum, Figure 4. The dash-dotted curve in Figure 7 is a schematic indication of such a maximum. Kim and Adrian (1999) argue that the motions that make up the low-frequency spectrum are a result of organized merging of small-scale motions.

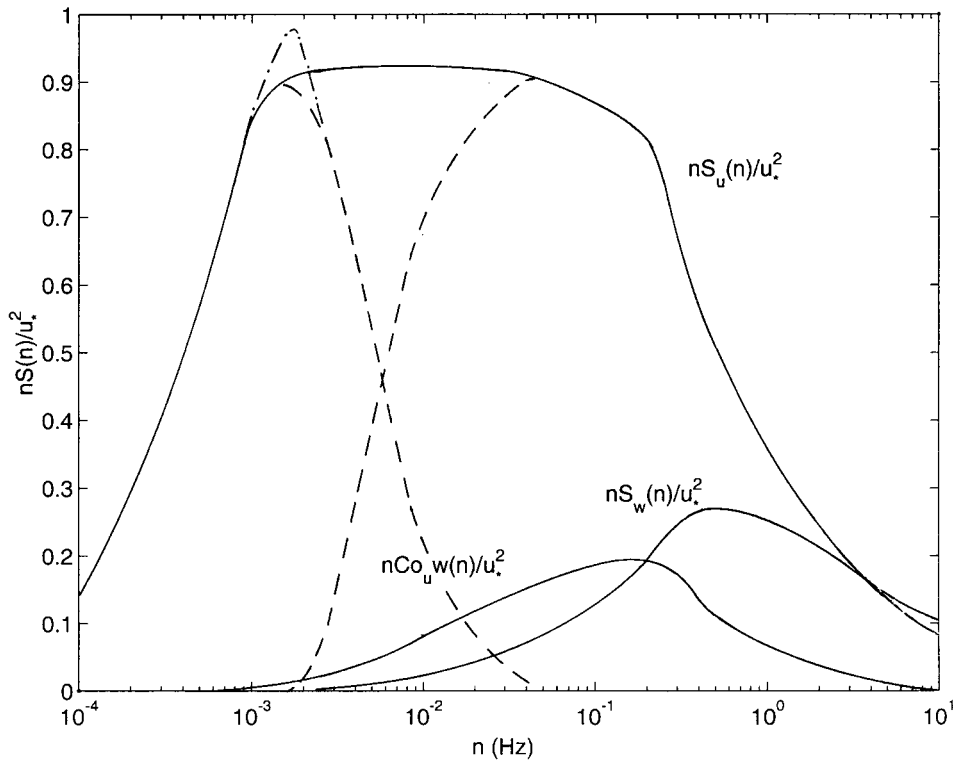


Figure 7. Example of normalized u and w spectra, $nS_u(n)/u_*^2$ and $nS_w(n)/u_*^2$ respectively, and uw cospectrum, $nCo_{uw}(n)/u_*^2$ in a representation with linear scale for spectral energy and logarithmic scale for frequency from the Lövsta site (Högström, 1990), 3 m. The full line curves are spectra derived from subjectively drawn best fit curves in log–log representation for one particular 30-minute period (4 June 1986, 1823 CET). The two dashed curves represent branches of possible spectral curves, the sum of which gives the observed u spectrum. The dash-dotted peak is a schematic representation of a spectral peak often observed in this position.

Large-eddy simulations of the neutral atmospheric boundary layer show very pronounced features, called ‘streaks’, which are strongly elongated in the streamwise direction and which occur in the lowest part of the boundary layer, see e.g., Moeng and Sullivan (1994) and Foster and Drobinski (2000). Although not explicitly mentioned in these papers, from the LES u -contour plots the typical length scale of these structures appears to be of the order of the boundary-layer depth or more. It is reasonable to assume that these streaks are identical to the VLSMs of the atmospheric case.

Moeng and Sullivan (1994) state that ‘the streaks are regions of concentrated large negative uw , which account for most of the Reynolds stress’. Foster and Drobinski (2000), on the other hand, find that streaks contribute to ten percent or less of the stress. From Figure 7 it is clear that the bulk of the momentum transport takes place on scales at least an order of magnitude less than the largest

scale. Högström and Bergström (1996) studied the momentum transport scales in near-neutral conditions at the Lövsta (Högström, 1990) and ‘Laban’s mills’ sites (Högström, 1992). Using the very effective detection method of Tiederman (1989), they identified bursts (events with upward flux of momentum deficit) and sweeps (events with downward transport of momentum excess) at heights ranging from 1.6 m to 14 m in the near-neutral surface layer. The mean duration of bursts and sweeps at the surface was found to be 4 to 5 seconds and the corresponding interval between two consecutive sweeps or bursts 10 to 14 seconds, these time intervals being independent of wind speed or friction velocity. Sweeps and bursts identified with this method were found to occur during 40 percent of the time, being, however, responsible for more than 90 percent of the momentum flux. Expressing the u and w fluctuations within every burst and sweep as the sum of a conditional mean for each identified structure, u_c and w_c respectively and a random fluctuation component, u' and w' , enabled identification of the flux contribution due to the organized motion within the structures, $\overline{u_c w_c}$, which was found to be more than 70 percent. The wind-speed independence of the observed characteristic time scales, δT , suggests that the corresponding alongwind scales, L are proportional to the neutral boundary-layer scale height u_*/f_c , so that, making the reasonable assumption that the structures are advected by the local mean wind,

$$L = \text{const. } u_*/f_c = \bar{u} \delta T. \quad (17)$$

Making use of the observed logarithmic wind profile and the observed mean time intervals quoted, shows that the constant is about 10^{-2} for the duration of bursts and sweeps near the surface, i.e., their length scale is identical to the length scale $L_e \approx h_e$. This means that the momentum transport process is likely to be strongly linked to the action of detached eddies as discussed in Section 2.1. This leads to the seemingly paradoxical conclusion that these ‘large’ eddies, which do, in fact, explain much of the features previously explained as the result of ‘inactive’ turbulence, are far from inactive, instead being the major carriers of the momentum transport. Note, that the eddies referred to here as ‘large’ are of the scale of the surface-layer height. The really large eddies in the surface layer, which are one to two orders of magnitude larger, are purely horizontal.

Conclusions

The various atmospheric neutral surface-layer characteristics identified by Högström (1990, 1992) as effects of ‘inactive’ turbulence are explained here in terms of ‘top-down’ mechanisms that dominate at high Reynolds number over the ‘bottom-up’ instability mechanisms that dominate at low Reynolds number. Detached eddies of relatively large scale, which are being brought down from above into the surface layer, cause the observed increase of dimensionless vertical velocity

variance with height as well as other ‘anomalies’ (as compared to traditional theory). As shown by the analysis of the height variation of σ_w^2/u_*^2 , the detached eddies are, however, of eddy-surface layer height scale and not of boundary-layer height scale. Most importantly, as shown in a previous study (Högström and Bergström, 1996), these eddies are a very effective means for momentum transport. This contrasts strongly to the statement of Townsend (1961) and Bradshaw (1967) that the ‘inactive’ eddies do not contribute to the shearing stress.

The high Reynolds number theory of Hunt and Morrison (2000), Hunt and Carloti (2001) predicts correctly not only the variation of σ_w^2/u_*^2 with height but also the low frequency fall-off of the dimensionless spectrum for the vertical velocity. The spectral level in this range is shown to be a factor of three higher than that given by the much quoted Kansas spectrum (Kaimal et al., 1972). Also the predictions for the cospectrum between u and w are verified by the measurements.

The dimensionless longitudinal velocity spectrum is also found to follow predictions from the high Reynolds number theory. This includes a spectral range with $nS_u(n)/u_*^2 \approx \gamma$, where $\gamma \approx 1$. The extension of this range in the frequency domain is shown to vary linearly with height z/h , where h is the height of the boundary layer. As $z/h \rightarrow 0$, the largest scale of the horizontal fluctuations $\Lambda_s \approx h$, and when $z/h \sim h_e/h$, $\Lambda_s = 3h$ near the top of the eddy surface layer. Above the eddy surface layer, i.e., for $z/h > h_e/h$, the magnitude of this scale decreases rapidly. This result is in qualitative accordance with the findings by Kim and Adrian (1999) from turbulent pipe flow, but differs in that Λ_s/h is of order one near the surface. They note that the ‘very large-scale motions’ (VLSMs) vary similarly with distance from the surface of the pipe. A recent analytical study by Foster (1997) and subsequent large-eddy simulation by the same author (Foster and Drobinski, 2000) indicate that the very large-scale structures of the atmospheric surface layer are probably identical to longitudinal streaks found in the logarithmic layer in these studies. They appear to be dynamically ‘preferred modes’ of neutral boundary-layer flow. In the atmospheric case they may result from organized merging of the originally detached eddies as they are being strongly deformed by blocking and shear close to the surface. These large eddies of obvious boundary-layer origin are found to be clearly separated from meso-scale motions at even larger scales. Thus, from an analysis of measurements over three periods with steady-state near-neutral conditions during several hours, a pronounced spectral minimum (‘spectral gap’) is found at a frequency around 7×10^{-4} Hz, the exact location being, however, dependent on measuring height and possibly other factors.

Acknowledgements

UH and AS were funded by a grant from the Swedish Natural Research Council (NFR) contract G5103-1340 and, partly, from EU-projects BASIS (MAS3-CT97-

0117) and SFINCS (ENV4-CT97-0573). JCRH thanks Uppsala University and the U.K. Met Office for supporting this research.

References

- BASIS: 2000, *Second Annual Report from the Meteorology Group, Uppsala University to the EU-project BALTIC-BASIS (Baltic Sea Ice Study)*, Contract No. MAS-CT97-0117.
- Bradshaw, P.: 1967L 'Inactive Motion and Pressure Fluctuations in Turbulent Boundary Layers', *J. Fluid Mech.* **30**(Part 2), 241–258.
- Coelho, S. L. V. and Hunt, J. C. R.: 1989, 'Vorticity Dynamics in the near Field of Strong Jets in Crossflows', *J. Fluid Mech.* **200**, 95–120.
- Davenport, A. G.: 1961, 'The Spectrum of Horizontal Gustiness near the Ground in High Wind Conditions', *Quart. J. Roy. Meteorol. Soc.* **87**, 194–211.
- Dyer, A. J.: 1974, 'A Review of Flux-Profile Relationships', *Boundary-Layer Meteorol.* **7**, 363–372.
- Falco, R. E.: 1982, 'A Synthesis and Model of Turbulence Structure in the Wall Region', in Zoran P. Zaric (ed.), *Structure of Turbulence in Heat and Mass Transfer*, Hemisphere Publ. Co., Washington.
- Foster, R. C.: 1997, 'Structure and Energetics of Optimal Ekman Layer Perturbations', *J. Fluid Mech.* **333**, 97–123.
- Foster, R. C. and Drobinski, P.: 2000, 'Near-Surface Streaks: Comparison of LES with Theory', in *Proceedings, 14th Symposium on Boundary Layers and Turbulence*, Aspen, Co, 7–11 August, 2000, pp. 499–502.
- Gage, K. S. and Nastrom, G. D.: 1986, 'Theoretical Interpretation of Atmospheric Wavenumber Spectra of Wind and Temperature Observed by Commercial Aircraft during GASP', *J. Atmos. Sci.* **43**, 729–740.
- Geernaert, G. L. and Plant, W. J.: 1990, *Surface Waves and Fluxes*, Vol. 1, *Current Theory*, Kluwer Academic Publishers, Norwell, MA, 336 pp.
- Haugen, D. A., Kaimal, J. C., and Bradley, E. F.: 1971, 'An Experimental Study of Reynolds Stress and Heat Flux in the Atmospheric Surface Layer', *Quart. J. Roy. Meteorol. Soc.* **97**, 168–180.
- Högström, U.: 1982, 'A Critical Evaluation of the Aerodynamical Error of a Turbulence Instrument', *J. Appl. Meteorol.* **21**, 1838–1844.
- Högström, U.: 1990, 'Analysis of Turbulence Structure in the Surface Layer with a Modified Similarity Theory Formulation for Neutral Conditions', *J. Atmos. Sci.* **47**, 1949–1972.
- Högström, U.: 1992, 'Further Evidence of Inactive Turbulence in the Near Neutral Atmospheric Surface Layer', in *Proceedings, 10th Symposium of Turbulence and Diffusion*, 29 Sept.–2 Oct. 1992, Portland, OR, pp. 188–191.
- Högström, U. and Bergström, H.: 1996, 'Organized Turbulence Structures in the Near-Neutral Surface Layer', *J. Atmos. Sci.* **53**, 2452–2464.
- Högström, U., Smedman, A., and Bergström, H.: 1999, 'A Case Study of Two-Dimensional Stratified Turbulence', *J. Atmos. Sci.* **56**, 959–976.
- Högström, U., Bergström, H., Smedman, A., Halldin, S., and Lindroth, A.: 1989, 'Turbulent Exchange above a Pine Forest. I: Fluxes and Gradients', *Boundary-Layer Meteorol.* **49**, 197–217.
- Hunt, J. C. R.: 1984, 'Turbulence Structure in Thermal Convection and Shear-Free Boundary Layers', *J. Fluid Mech.* **138**, 161–184.
- Hunt, J. C. R. and Carlotti, P.: 2001, 'Statistical Structure of the High Reynolds Number Turbulent Boundary Layer', *Flow, Turbulence, Combustion*, in press.
- Hunt, J. C. R. and Durbin, P. A.: 1999, 'Perturbed Vortical Layers and Shear Sheltering', *Fluid Dyn. Res.* **24**, 375–404.

- Hunt, J. C. R. and Morrison, J. F.: 2000, 'Eddy Structure in Turbulent Boundary Layers', *Euro J. Mech. B – Fluids* **19**, 673–694.
- Hunt, J. C. R., Moin, P., Lee, M., Moser, R. D., Spalart, P., Mansour, N. N., Kaimal, J. C., and Gaynor, E.: 1989, 'Cross Correlations and Length Scales in Turbulent Flows near Surfaces', in H. Fiedler and H. Fernholz (eds.), *Advances in Turbulence*, Vol. 2, Springer-Verlag, pp. 128–134.
- Johansson, C., Smedman, A., Höögström, U., Brasseur, J. G., and Khanna, S.: 2001, 'Critical Test of Monin–Obukhov Similarity during Convective Conditions', *J. Atmos. Sci.* **58**, 1549–1566.
- Kaimal, J. C., Wyngaard, J. C., Izumi, Y., and Coté, O. R.: 1972, 'Spectral Characteristics of Surface-Layer Turbulence', *Quart. J. Roy. Meteorol. Soc.* **98**, 563–589.
- Katul, G. and Chu, C.-R.: 1998, 'A Theoretical and Experimental Investigation on Energy-Containing Scales in the Dynamic Sublayer of Boundary-Layer Flows', *Boundary-Layer Meteorol.* **86**, 279–312.
- Kim, K. C. and Adrian, R. J.: 1999, 'Very Large-Scale Motion in the Outer Layer', *Phys. Fluids* **11**, 417–422.
- Mann, J.: 1994, 'The Spatial Structure of Neutral Atmospheric Surface-Layer Turbulence', *J. Fluid Mech.* **273**, 141–168.
- Marusic, I. and Perry, A. E.: 1995, 'A Wake Model for the Turbulence Structure of Boundary Layers. Part 2. Further Experimental Support', *J. Fluid Mech.* **298**, 389–407.
- Moeng, C.-H. and Sullivan, P. P.: 1994, 'A Comparison of Shear- and Buoyancy-Driven Planetary Boundary Layer Flow', *J. Atmos. Sci.* **51**, 999–1022.
- Monin, A. S. and Yaglom, A. M.: 1971, *Statistical Fluid Mechanics*, Vol. 1, English translation, The MIT Press, Cambridge, MA, 769 pp.
- Panofsky, H. A.: 1969, 'Spectra of Atmospheric Variables in the Boundary Layer', *Radio Sci.* **4**, 1101–1109.
- Panofsky, H. A., Tennekes, H., Lenschow, D. H., and Wyngaard, J. C.: 1977, 'The Characteristics of Turbulent Velocity Components in the Surface Layer under Convective Conditions', *Boundary-Layer Meteorol.* **11**, 355–361.
- Perot, B. and Moin, P.: 1995, 'Shear-Free Turbulent Boundary Layers. Part 1. Physical Insights into Near-Wall Turbulence', *J. Fluid Mech.* **295**, 199–227.
- Perry, A. E. and Abell, C. J.: 1977, 'Asymptotic Similarity of Turbulence Structures in Smooth- and Rough-Walled Pipes', *J. Fluid Mech.* **79**, 785–789.
- Perry, A. E., Henbest, S., and Chong, M. S.: 1986, 'A Theoretical and Experimental Study of Wall Turbulence', *J. Fluid Mech.* **165**, 163–199.
- Robinson, S. K.: 1991, *The Kinematics of Turbulent Boundary Layer Structure*, NASA Technical Memo. 103859, Ames Research Center, Moffet Field, CA, 479 pp.
- Sandham, N. D. and Kleiser, L.: 1992, 'The Late Stages of Transition to Turbulence in Channel Flow', *J. Fluid Mech.* **245**, 319–348.
- Smedman, A.: 1991a, 'Some Turbulence Characteristics in Stable Atmospheric Boundary Layer Flow', *J. Atmos. Sci.* **48**, 856–868.
- Smedman, A.: 1991b, 'Occurrence of Roll Circulations in a Shallow Boundary Layer', *Boundary-Layer Meteorol.* **57**, 343–358.
- Smedman, A., Höögström, U., Bergström, H., Rutgerson, A., Kahma, K. K., and Pettersson, H.: 1999, 'A Case Study of Air–Sea Interaction during Swell Conditions', *J. Geophys. Res.* **104**, 25,833–25,851.
- Smedman, A., Tjernström, M., and Höögström, U.: 1994, 'The Near-Neutral Marine Atmospheric Boundary Layer with No Surface Shearing Stress: A Case Study', *J. Atmos. Sci.* **51**, 3399–3411.
- Smedman-Höögström, A. and Höögström, U.: 1975, 'Spectral Gap in Surface-Layer Measurements', *J. Atmos. Sci.* **32**, 340–350.
- Smith, S. D. and Banke, E. G.: 1975, 'Variation of the Sea Surface Drag Coefficient with Wind Speed', *Quart. J. Roy. Meteorol. Soc.* **101**, 665–673.

- Spalart, P. R.: 1988, 'Direct Numerical Simulation of a Turbulent Boundary Layer up to $Re_\theta = 1410$ ', *J. Fluid Mech.* **187**, 61–98.
- Tiederman, W. G.: 1989, 'Eulerian Detection of Turbulent Bursts', in S. J. Kline and N. H. Afgan (eds.), *Near Wall Turbulence. Proceedings of the Z. Zoriac Memorial Conference 1988*, Hemisphere, pp. 874–887.
- Townsend, A. A.: 1961, 'Equilibrium Layers and Wall Turbulence', *J. Fluid Mech.* **11**, 97–120.
- Townsend, A. A.: 1976, *The Structure of Turbulent Shear Flow*, 2nd edn., Cambridge University Press, Cambridge, 429 pp.
- Wyngaard, J. C. and Coté, O. R.: 1972, 'Cospectral Similarity in the Atmospheric Surface Layer', *Quart. J. Roy. Meteorol. Soc.* **98**, 590–603.